*remote sensing*

MDPI

*Article*

# Seasonal and Elevational Variations of Forest Greenness in Changbai Mountain During 2000–2024

**Yan Wang [1,2], Zhiping Zhao [1,*], Zhuoqing Li [1] and Chaoyang Feng [1]**

[1] Institute of Ecology, Chinese Research Academy of Environmental Sciences, Beijing 100012, China; wangyan2024@lzu.edu.cn (Y.W.); li.zhuoqing@craes.org.cn (Z.L.); fengchy@craes.org.cn (C.F.)
[2] College of Ecology, Lanzhou University, Lanzhou 730000, China
* Correspondence: zhaozhiping@craes.org.cn

## Highlights

### What are the main findings?

- Seasonal differences were observed in forest greenness trends, with autumn showing the largest estimated NDVI slope.
- Spring NDVI showed the highest temperature correlation among seasons.
- Climate–greenness correlations differed among seasons and elevation zones, and spring correlations varied over time.
- A significant positive NTL–NDVI association was detected only at low elevation.

### What are the implications of the main findings?

- Seasonal and elevational analyses help identify contrasting greenness responses masked by growing-season averages.
- NTL–NDVI associations should be interpreted cautiously because nighttime light integrates multiple human-related illumination sources.

## Abstract

Mountain forest greenness varies across seasons, yet growing-season averages can mask season-specific relationships with climate variability. We assessed seasonal and elevational variation in historical forest greenness within areas classified as forest in 2024, temporal variation in spring NDVI–climate relationships, and the association between nighttime light (NTL) intensity and forest greenness in Changbai Mountain from 2000 to 2024. We used MODIS-derived normalized difference vegetation index (NDVI), 1 km temperature and precipitation datasets, elevation zones, and annual nighttime light (NTL) data. We applied a forest mask derived from the 2024 Annual China Land Cover Dataset (CLCD) and retained 1 km pixels with at least 70% forest cover. NDVI increased significantly over the aggregate growing season (slope = 0.0011 NDVI $yr^{-1}$, $R^2 = 0.584$, $p < 0.001$), summer (slope = 0.0006 NDVI $yr^{-1}$, $R^2 = 0.188$, $p = 0.030$), and autumn (slope = 0.0019 NDVI $yr^{-1}$, $R^2 = 0.280$, $p = 0.007$). Autumn showed the largest estimated slope; this ranking alone does not establish statistical differences among seasonal slopes. Spring showed no significant long-term trend (slope = 0.0011 NDVI $yr^{-1}$, $R^2 = 0.087$, $p = 0.152$), but spring NDVI showed a strong positive correlation with temperature at the regional scale ($r = 0.760$, $p < 0.001$), with positive correlations maintained across all elevation zones. In spring regression models, temperature showed a larger standardized coefficient magnitude than precipitation across elevation zones, with all variance inflation factors $\leq 1.22$. Exploratory five-year sliding-window correlations suggested temporal variation in spring NDVI–climate relationships, although each estimate was based on only five annual observations. At low elevation, the NTL–NDVI regression was significant ($R^2 = 0.198$, $p = 0.026$), whereas associations at

Check for updates

Academic Editor: Huaqiang Du

Received: 28 September 2026
Revised: 15 October 2026
Accepted: 19 October 2026
Published: 22 October 2026

**Copyright:** © 2026 by the authors. Licensee MDPI, Basel, Switzerland. This article is an open access article distributed under the terms and conditions of the Creative Commons Attribution (CC BY) license.

middle and high elevations were not statistically significant; this raw association should be interpreted cautiously because both variables may contain concurrent temporal trends. These results describe seasonal and elevational greenness patterns within the 2024 forest mask, highlighting the distinct spring temperature association and elevation-dependent relationships between NTL intensity and forest greenness.

**Keywords:** NDVI; mountain forests; seasonal greenness; elevation gradient; nighttime light; Changbai Mountain

## 1. Introduction

Mountain forests are particularly sensitive to climate variability because topography compresses gradients in temperature, moisture, snow conditions, and growing-season length over short distances [1–3]. Satellite observations have documented widespread vegetation greening in many regions [4], but regional-scale trends provide limited insight into how forest greenness varies among seasons and elevation zones [5,6]. Along mountain slopes, climatic conditions and vegetation responses can differ across phenological stages, resulting in seasonal and elevational variation in vegetation dynamics [3,5,7].

Growing-season averages are widely used for vegetation monitoring, but they may obscure seasonal differences in vegetation responses [6]. Spring canopy development is commonly associated with heat accumulation, snowmelt processes, and soil thawing [2,3,8,9], whereas autumn greenness may reflect variation in senescence timing and late-season canopy activity [2,6]. Therefore, seasonal analyses are needed to better characterize temporal differences in forest greenness dynamics and their relationships with environmental variability [10].

Elevation gradients integrate differences in temperature, snow persistence, growing-season length, vegetation phenology, forest composition, and human accessibility, providing natural environmental contrasts over relatively short geographic distances. Elevation-dependent vegetation responses have been reported across mountain systems [5]. Changbai Mountain is characterized by pronounced vertical forest zonation over a relatively short geographic distance [11], together with vegetation dynamics associated with climate variability [12–14]. This natural elevational gradient provides a framework for comparing seasonal greenness patterns and climate associations across forest zones with contrasting thermal, snow, and phenological conditions [3,8,11].

The combination of vertical forest zonation, seasonal snow processes, and contrasting accessibility makes Changbai Mountain suitable for examining multiple controls on forest greenness. Spring canopy development in this region is closely associated with temperature and snowmelt processes, whereas autumn greenness reflects late-season vegetation activity and senescence dynamics [3,6,8]. Differences in accessibility between lower- and higher-elevation forests also provide a spatial gradient for assessing relationships between landscape-scale human-related indicators and vegetation greenness. Together, these characteristics allow seasonal, elevational, and human-related influences on forest greenness to be examined within a single mountain ecosystem.

Climate–NDVI relationships may also vary over time. Correlations calculated over an entire study period describe average relationships but may obscure temporal fluctuations in the strength or direction of these associations [15]. Sliding-window correlations provide an approach for exploring temporal variation in climate–vegetation relationships [15], although estimates based on short and overlapping windows require cautious interpretation because individual years may influence multiple consecutive windows.

Nighttime light (NTL) data provide a spatial indicator of artificial illumination associated with human presence and socioeconomic activity [16–18]. In forested mountain regions, NTL may provide contextual information on spatial variation in human-related activity patterns, particularly in lower-elevation landscapes where accessibility and infrastructure are generally greater. However, NTL signals represent landscape-scale illumination and may include contributions from nearby settlements, roads, tourism facilities, and other artificial light sources rather than directly measuring activity within forest stands [6,17]. Therefore, NTL–vegetation relationships should be interpreted considering the spatial context represented by these signals.

Changbai Mountain has been investigated in previous studies focusing on seasonal vegetation dynamics across Northeast China [6] and vegetation dynamics, forest phenology, and climate associations specifically within the region [3,8]. However, few studies have jointly examined seasonal, elevational, temporal, and human-related dimensions of forest greenness within the same mountain landscape. Building on previous research, we used a fixed forest mask derived from the 2024 Annual China Land Cover Dataset (CLCD) to define a consistent spatial framework for long-term analysis. This approach allowed us to examine historical greenness trajectories within forest areas identified in 2024 rather than changes in forest extent or forest-cover transitions during the study period. We combined seasonal and elevation-stratified analyses, sliding-window spring climate correlations, and NTL–NDVI regression analyses to investigate seasonal, elevational, and temporal variation in forest greenness and its statistical relationships with climate variability and landscape-scale human-related indicators. This framework was designed to describe observed patterns and associations rather than infer specific causal mechanisms. The regional contribution is the joint characterization of seasonal and elevational greenness dynamics over an extended satellite record, together with an assessment of how landscape-scale human-related indicators are associated with forest greenness across elevation zones.

Specifically, we address four questions: (1) How did forest greenness within areas classified as forest in 2024 change during spring, summer, autumn, and the aggregate growing season (April–October) from 2000 to 2024? (2) How did seasonal NDVI associations with temperature and precipitation vary across elevation zones in Changbai Mountain? (3) Did spring climate–NDVI associations vary over time based on sliding-window analyses? (4) How did the association between NTL intensity and growing-season NDVI vary among elevation zones?

## 2. Materials and Methods

### 2.1. Study Area

The study area is located within the Changbai Mountain Protection and Development Zone in northeastern China and covers parts of Antu County, Fusong County, and Changbai Korean Autonomous County (Figure 1). It covers approximately 3500 km$^2$ and extends from 127°28′ to 128°16′E and from 41°42′ to 42°25′N. Elevation ranges from approximately 600 to 2700 m, creating pronounced gradients in temperature, moisture, snow conditions, and phenology over short distances.

The region experiences a temperate monsoon climate, with most annual precipitation occurring from June to September. Forest vegetation exhibits clear vertical zonation. Korean pine–broad-leaved mixed forest predominates at lower elevations, dark coniferous forest occupies the middle-elevation belt, and Erman's birch forest occurs near the upper forest limit, with alpine tundra above the forest belt. The thresholds of 1100 and 1700 m broadly correspond to the major transitions among the Korean pine–broad-leaved mixed forest, dark coniferous forest, and Erman's birch forest belts [11]. Together, the vertical vegetation zonation and climatic gradients provide a natural setting for comparing seasonal greenness

and its climate associations among elevation zones. For the elevation-stratified analyses, forest pixels were classified into three zones: low (<1100 m), middle (1100–1700 m), and high (>1700 m).

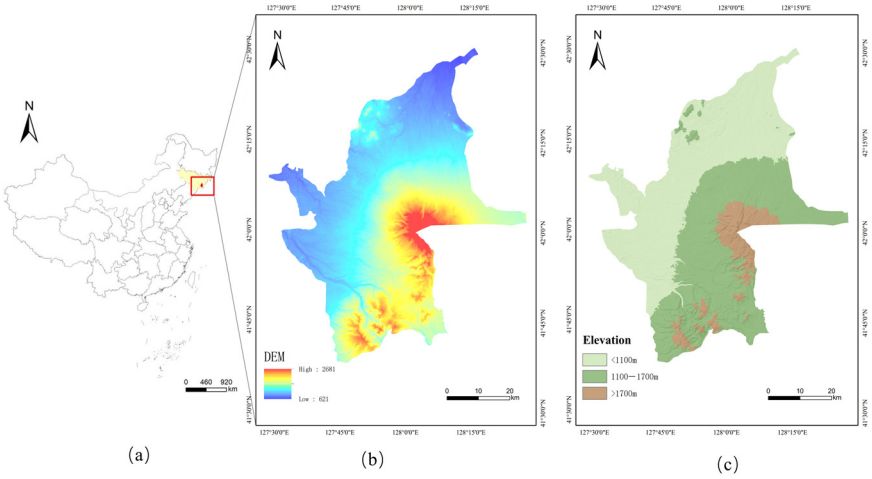


**Figure 1.** Location, topography, and elevation zones of the study area in Changbai Mountain. (**a**) Regional location of the study area in northeastern China. (**b**) Continuous elevation map derived from a digital elevation model (DEM) within the forest mask. (**c**) Spatial distribution of low (<1100 m), middle (1100–1700 m), and high (>1700 m) elevation zones within the forest mask. Elevations are expressed in meters.

The close juxtaposition of forest belts along this mountain gradient provides environmental contrasts in temperature, snow persistence, phenological timing, and growing-season length [3,8,11]. This setting allows seasonal climate–greenness associations to be compared among elevation zones within the same regional landscape.

### 2.2. Data Sources

We compiled vegetation index, climate, land-cover, nighttime light (NTL), and elevation data for the period 2000–2024 (Table 1).

**Table 1.** Data sources, versions and analytical roles.

| Data Type | Dataset/Product | Period | Temporal Resolution | Spatial Resolution | Role |
|---|---|---|---|---|---|
| NDVI | MODIS/Terra MOD13A3 V061 | 2000–2024 | Monthly | 1 km | Forest greenness |
| Land cover | Annual China Land Cover Dataset (CLCD) v01, Version 1.0.4; | 2024 | Static classification | 30 m | 70% forest mask; Forest class code 2 |
| Temperature | 1 km Monthly Mean Temperature Dataset for China | 2000–2024 | Monthly | 1 km | Climate association |
| Precipitation | 1 km Monthly Precipitation Dataset for China | 2000–2024 | Monthly | 1 km | Climate association |
| NTL | Extended NPP-VIIRS-like nighttime light dataset for China | 2000–2024 | Annual | 500 m | Nighttime-light-derived signal |
| Elevation | ASTER GDEM V003 | Static | Static | 30 m | Elevation zones |

Vegetation data were obtained from the MODIS/Terra Vegetation Indices Monthly L3 Global 1 km product (MOD13A3, Version 6.1) via Google Earth Engine [19]. MODIS vegetation indices have been widely applied for monitoring vegetation dynamics due to their consistent radiometric quality and long-term temporal coverage [20]. This product provides monthly normalized difference vegetation index (NDVI) observations at 1 km spatial resolution.

Monthly mean temperature and precipitation data for 2000–2024 were obtained from the 1 km Monthly Mean Temperature Dataset for China and the 1 km Monthly Precipitation Dataset for China, respectively. Both datasets were provided by the National Tibetan Plateau/Third Pole Environment Data Center [21,22].

Annual NTL data for 2000–2024 were obtained from the Extended VIIRS-Like Artificial Nighttime Light Dataset of China, provided by the National Tibetan Plateau/Third Pole Environment Data Center [23]. The annual NTL rasters were aligned with the common analysis grid before mean values were calculated for each elevation zone.

Land-cover information was obtained from the 2024 Annual China Land Cover Dataset (CLCD) v01, Version 1.0.4, developed by Jie Yang and Xin Huang at Wuhan University and distributed through Zenodo [24]. The CLCD was derived from Landsat surface reflectance using random forest classification, spatiotemporal filtering, and logical post-processing. Forest was represented by class code 2, and the 2024 raster covering the study area was used to construct the forest-cover mask.

Elevation data were obtained from the ASTER Global Digital Elevation Model Version 3 (ASTER GDEM V003), provided by the Geospatial Data Cloud [25]. The dataset has a spatial resolution of 30 m and was used to derive elevation information.

### *2.3. Forest Mask and Spatial Harmonisation*

The 2024 Annual China Land Cover Dataset (CLCD v01, Version 1.0.4) was used to construct the forest mask. The CLCD raster was supplied in an Albers Equal-Area Conic projection based on the WGS 1984 datum [24].

Forest cover was quantified from source-pixel areas rather than by assigning a single land-cover class to each MODIS pixel through majority-rule or nearest-neighbour resampling. Forest pixels were first identified at the native 30 m CLCD resolution. For each source pixel, forest area and valid classified area were calculated separately and then aggregated independently to the MODIS NDVI grid by area summation. The forest-cover proportion of each MODIS pixel was calculated as

$$F_i = \frac{\sum_{j \in S_i} I_j A_j}{\sum_{j \in S_i} V_j A_j}, \tag{1}$$

where $F_i$ is the forest-cover proportion of MODIS pixel $i$; $S_i$ is the set of 30 m source pixels assigned to MODIS pixel $i$ during spatial aggregation; $I_j$ is the forest indicator for source pixel $j$, with forest pixels assigned a value of 1 and all other valid land-cover classes assigned a value of 0; $V_j$ is the valid-classification indicator, with valid land-cover pixels assigned a value of 1 and NoData pixels assigned a value of 0; and $A_j$ is the actual area of source pixel $j$.

The forest mask was defined as

$$\mathrm{M_i} = \begin{cases} 1, & \mathrm{F_i} \geq 0.70, \\ \mathrm{NA}, & \mathrm{F_i} < 0.70, \end{cases} \tag{2}$$

where $\mathrm{M_i} = 1$ denotes a retained forest pixel and $\mathrm{M_i} = \mathrm{NA}$ denotes a pixel excluded from subsequent analyses. The final mask retained MODIS pixels in which forest accounted for at least 70% of the area with valid 2024 CLCD classifications. This criterion limited

the combined non-forest fraction to at most 30% of the valid classified area within each retained pixel. Because the subsequent analyses focused on forest vegetation, forest fraction was used to screen mixed pixels, and the non-forest fraction was not further disaggregated by land-cover class. This fixed reference-year mask was applied consistently to all NDVI, climate, and NTL analyses throughout the 2000–2024 study period to maintain a constant spatial framework for temporal comparisons. Bartold [26] applied a reference-year forest mask to a multiyear vegetation-index record, providing a precedent for a fixed spatial domain without establishing historical forest-cover persistence. Similar fixed forest-domain approaches have also been widely applied in satellite-based forest monitoring to maintain consistent spatial definitions across time series analyses [27]. Accordingly, this study investigates historical greenness trajectories within areas classified as forest in 2024 rather than changes in total forest extent or forest-cover transitions during the study period.

The 70% threshold was selected by comparing candidate forest masks within the study area. A 50% threshold retained 4627 MODIS pixels and 3433.53 km$^2$ of CLCD-derived forest area, whereas the 70% threshold retained 4568 pixels and 3389.78 km$^2$. Increasing the threshold removed 59 pixels and 43.75 km$^2$ of forest area while retaining 98.73% of the pixels identified under the 50% criterion. The 70% threshold therefore increased the minimum forest proportion of retained pixels while excluding only a limited proportion of candidate forest area. It was treated as a study-specific screening criterion rather than a universal remote-sensing standard or statistical threshold. The resulting forest mask is shown in Figure 2.

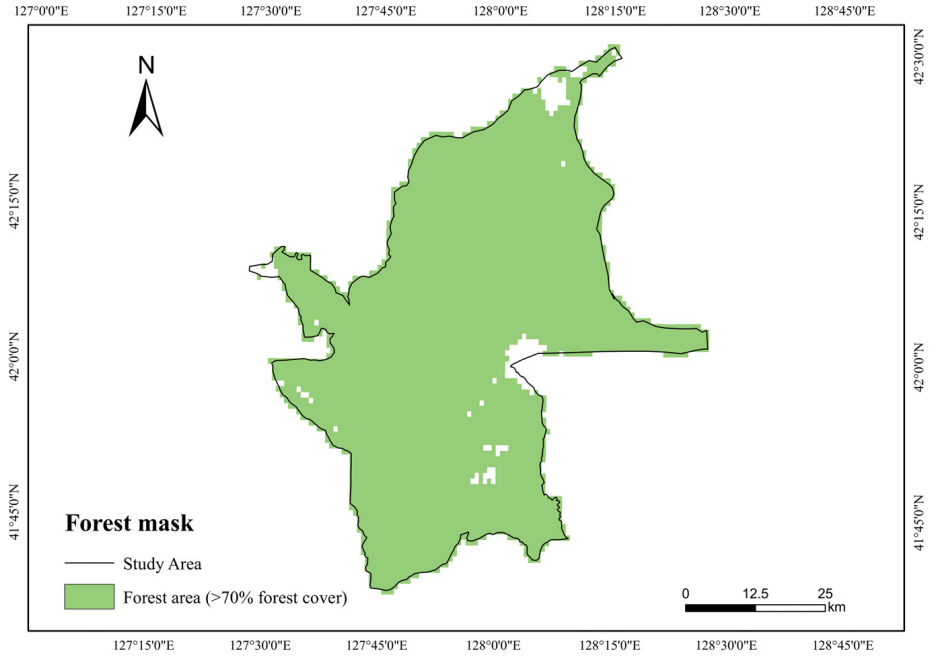


**Figure 2.** Spatial distribution of the forest mask in Changbai Mountain. The mask was derived from the 2024 Annual China Land Cover Dataset (CLCD), retaining 1 km MODIS pixels in which forest accounted for at least 70% of the valid classified area. Green shading indicates the retained MODIS pixels, and the black outline indicates the study area boundary.

After assignment to the elevation zones, the final elevation-stratified sample comprised 4344 forest pixels and 3223.62 km$^2$ of CLCD-derived masked forest area (Table 2). Low- and middle-elevation zones accounted for 47.64% and 44.54% of the masked forest area, respectively, whereas the high-elevation zone accounted for 7.82%.

**Table 2.** Forest-pixel counts and CLCD-based forest area by elevation zone used for elevation-stratified analyses.

| Elevation Zone | Forest-Pixel Count | Forest Area (km$^2$) | Percentage of Total Masked Forest Area |
|---|---|---|---|
| Low elevation (<1100 m) | 2073 | 1535.77 | 47.64% |
| Middle elevation (1100–1700 m) | 1932 | 1435.81 | 44.54% |
| High elevation (>1700 m) | 339 | 252.05 | 7.82% |
| Total | 4344 | 3223.62 | 100.00% |

MODIS NDVI defined the common analysis grid and was not resampled. The forest mask and DEM-derived elevation zones, both categorical layers, were aligned to the MODIS grid using nearest-neighbour assignment. Temperature and precipitation, as continuous variables, were aligned using bilinear interpolation. Annual NTL rasters were aligned to the same analysis grid before zonal means were calculated.

Area-weighted means were calculated for the entire masked forest area and for each elevation zone as

$$\bar{X}_{y,z} = \frac{\sum_{i \in Z_z} X_{i,y} A_i}{\sum_{i \in Z_z} A_i}, \quad (3)$$

where $\bar{X}_{y,z}$ is the area-weighted mean for year $y$ and spatial zone $z$; $Z_z$ is the set of valid forest pixels within zone $z$; $X_{i,y}$ is the temperature, precipitation, or NTL value of pixel $i$ in year $y$; and $A_i$ is the actual area of pixel $i$. The spatial zone $z$ represents either the entire masked forest area or one of the three elevation zones. Area weighting was used to account for differences in the actual area represented by geographic-grid pixels at different latitudes.

### *2.4. Seasonal Aggregation and Data Completeness*

Seasonal periods were defined a priori before statistical analyses as follows: the growing season was defined as April–October, spring as April–May, summer as June–August, and autumn as September–October. The growing-season metric was analysed separately as an aggregate period spanning the three seasonal windows; therefore, it was not independent of the individual seasonal metrics. The fixed calendar windows distinguish early-season, summer, and late-season greenness in the local phenological context [3,7,8]; they do not represent annually observed phenological transition dates for each elevation zone.

For year $y$ and seasonal period $s$, seasonal mean NDVI was calculated as

$$\left( \mathrm{NDVI}_{y,s} = \frac{1}{n_s} \sum_{m \in s} \mathrm{NDVI}_{y,m} \right), \quad (4)$$

where $\mathrm{NDVI}_{y,s}$ is the mean NDVI for seasonal period $s$ in year $y$, $\mathrm{NDVI}_{y,m}$ is the monthly NDVI in month $m$, and $n_s$ is the number of months included in seasonal period $s$.

Seasonal mean temperature was calculated as

$$\left( T_{y,s} = \frac{1}{n_s} \sum_{m \in s} T_{y,m} \right), \quad (5)$$

where $T_{y,s}$ is the mean temperature for seasonal period $s$ in year $y$, and $T_{y,m}$ is the monthly mean temperature in month $m$.

Seasonal precipitation was calculated as the sum of monthly precipitation:

$$P_{y,s} = \sum_{m \in s} P_{y,m}, \quad (6)$$

where $P_{y,s}$ is the total precipitation for seasonal period $s$ in year $y$, and $P_{y,m}$ is the monthly total precipitation in month $m$. Annual NTL data required no temporal aggregation.

The fixed 2024 CLCD-derived forest mask and the same elevation zones were applied throughout 2000–2024 to characterize temporal variations in vegetation and climate relationships within the 2024 forest mask. Seasonal values were calculated only when observations were available for all constituent months. The final dataset contained 25 complete annual observations for each seasonal period and spatial unit. Spatial means for the entire masked forest area and for each elevation zone were calculated using the area-weighting procedure described in Section 2.3.

### *2.5. Statistical Analyses*

#### 2.5.1. Seasonal NDVI Trends

Long-term trends in spring, summer, and autumn NDVI, as well as aggregate growing-season NDVI, from 2000 to 2024 were quantified using ordinary least squares (OLS) regression, a widely used method for analyzing temporal trends in satellite-derived vegetation indices [28]:

$$\mathrm{NDVI}_{y,s} = \alpha_s + \beta_s t_y + \varepsilon_{y,s}, \quad (7)$$

where $\mathrm{NDVI}_{y,s}$ is the mean NDVI for seasonal period $s$ in year $y$, $t_y$ is the corresponding calendar year, $\alpha_s$ is the intercept, $\beta_s$ is the annual rate of NDVI change, and $\varepsilon_{y,s}$ is the residual error. Trend direction and magnitude were evaluated using the regression slope, coefficient of determination ($R^2$), and $p$-value for $\beta_s$.

Growing-season NDVI (April–October) integrates spring, summer, and autumn and is therefore statistically non-independent of these seasonal metrics. Its separately fitted ordinary least-squares trend is interpreted as an aggregate summary, not as a fourth independent seasonal response.

To compare NDVI trends among different seasonal periods, a linear model including year, period, and their interaction was fitted:

$$NDVI_{i,t} = \beta_0 + \beta_1 Year_t + \beta_2 Season_i + \beta_3 (Year_t \times Season_i) + \epsilon$$

where $NDVI_{i,t}$ represents NDVI in period $i$ and year $t$; $Year_t$ denotes the observation year; and $Period_i$ is a categorical variable representing four NDVI periods (spring, summer, autumn, and growing season). The year × period interaction term tested whether the rate of change in NDVI differed among periods. Period-specific trend slopes were derived using the emtrends function in the emmeans package, and pairwise comparisons of slopes were performed with Tukey adjustment.

#### 2.5.2. NDVI–Climate Correlations and Standardized Regression

Pearson correlation coefficients were calculated between seasonal NDVI and concurrent seasonal mean temperature and between seasonal NDVI and concurrent seasonal total precipitation. Correlations were first calculated for the entire masked forest area and then separately for the low-, middle-, and high-elevation zones. These concurrent-season analyses describe synchronous associations and do not test antecedent, lagged, or cumulative climate relationships.

For two annual variables $x$ and $y$, the Pearson correlation coefficient was calculated as

$$r = \frac{\sum_{i=1}^{n}(x_i - \bar{x})(y_i - \bar{y})}{\sqrt{\sum_{i=1}^{n}(x_i - \bar{x})^2}\sqrt{\sum_{i=1}^{n}(y_i - \bar{y})^2}}, \quad (8)$$

where $x_i$ and $y_i$ are the paired NDVI and climate observations in year $i$, $\bar{x}$ and $\bar{y}$ are their respective means, and $n$ is the number of paired observations. Each full-period correlation was based on 25 annual observations. Correlation coefficients, two-sided $p$-values, and sample sizes were reported.

To compare the relative magnitudes of temperature and precipitation coefficients within each seasonal period and elevation zone, NDVI, temperature, and precipitation were standardized as follows:

$$z(X) = \frac{X - \bar{X}}{\mathrm{SD}(X)}, \quad (9)$$

where $X$ denotes NDVI, temperature, or precipitation, $\bar{X}$ is its mean, and SD($X$) is its standard deviation.

A standardized multiple linear regression model was then fitted:

$$z(\mathrm{NDVI}) = \alpha + \beta_T z(T) + \beta_P z(P) + \varepsilon, \quad (10)$$

where T and P denote temperature and precipitation, respectively; $\alpha$ is the intercept; $\beta$T and $\beta$P are the standardized regression coefficients for temperature and precipitation; and $\varepsilon$ is the residual error.

The relative magnitude of the standardized temperature coefficient was calculated as

$$C_T = \frac{|\beta_T|}{|\beta_T| + |\beta_P|} \times 100\%, \quad (11)$$

whereas the relative magnitude of the standardized precipitation coefficient was calculated as

$$C_P = \frac{|\beta_P|}{|\beta_T| + |\beta_P|} \times 100\%. \quad (12)$$

The signs of $\beta_T$ and $\beta_P$ were retained when interpreting the direction of each relationship, whereas their absolute values were used only to calculate the relative magnitudes of the standardized coefficients. These percentages represent the relative magnitude of the two standardized coefficients within the same model and should not be interpreted as independent variance decomposition, explained variance, or causal contributions to NDVI variability.

Multicollinearity between temperature and precipitation was assessed using the variance inflation factor:

$$\mathrm{VIF} = \frac{1}{1 - r_{TP}^2}, \quad (13)$$

where $r_{TP}$ is the Pearson correlation coefficient between temperature and precipitation. VIF values below 5 were considered to indicate no problematic multicollinearity [29].

#### 2.5.3. Sliding-Window Correlations

The spring NDVI–climate correlation estimates reported here were examined using 5-year sliding windows following satellite time-series approaches that use moving-window analyses to evaluate temporal changes in vegetation dynamics [30]. Each correlation

estimate was based on five annual observations, and adjacent windows shared four years. For a window beginning in year $t$, the included annual observations were defined as

$$W_t = \{t, t+1, t+2, t+3, t+4\}, \tag{14}$$

and the corresponding center year was calculated as

$$c_t = t + 2. \tag{15}$$

The first window covered 2000–2004 and was represented by the center year 2002, whereas the final window covered 2020–2024 and was represented by 2022. This procedure produced 21 overlapping windows.

Within each window, Pearson correlation coefficients were calculated between NDVI and temperature and between NDVI and precipitation. A correlation coefficient was calculated when complete paired annual observations were available within each moving window.

An additional 10-year sliding-window analysis was conducted to examine sensitivity of correlation patterns to window length. The results were compared with the five-year analysis to assess whether the observed temporal variations were consistent across window lengths.

The sliding-window analysis was used to explore variation in the strength and direction of correlation estimates among overlapping windows, without identifying dated ecological transitions.

#### 2.5.4. NTL–NDVI Regression Analysis

The NTL analysis was designed to evaluate the association between a landscape-scale human-related indicator and vegetation dynamics across elevation zones. Annual mean NTL and growing-season NDVI were summarized within the same forest-dominated areas and elevation zones. The analyses were restricted to the forest mask defined in Section 2.3 (pixels with forest coverage $\geq 70\%$). Annual NTL data covered the same period (2000–2024) as the NDVI and climate datasets. NTL represents landscape-scale illumination signals associated with human presence [31]. In forest-dominated pixels, these signals may include lights from the non-forest fraction and illumination from nearby roads, settlements, or tourism facilities, including light spill; they do not directly measure activity within forest stands [16,17].

For each elevation zone, the relationship between NTL intensity and growing-season NDVI was evaluated using ordinary least-squares regression:

$$\mathrm{NDVI}_y = \alpha + \gamma \mathrm{NTL}_y + \varepsilon_y, \tag{16}$$

where $\mathrm{NDVI}_y$ is growing-season mean NDVI in year $y$, $\mathrm{NTL}_y$ is annual mean nighttime light intensity in the same year and elevation zone, $\alpha$ is the intercept, $\gamma$ is the regression coefficient, and $\varepsilon_y$ is the residual error. Each elevation-specific regression was based on 25 annual observations.

All statistical analyses were conducted in R version 4.4.1. Unless otherwise stated, statistical tests were two-sided, and $p < 0.05$ was considered statistically significant.

## 3. Results

### *3.1. Seasonal NDVI Trends from 2000 to 2024*

From 2000 to 2024, NDVI trends were positive in spring, summer, autumn, and the growing season overall, although not all trends were statistically significant (Figure 3).

Autumn had the largest estimated seasonal slope (slope = 0.0019 NDVI $yr^{-1}$, $R^2$ = 0.280, $p$ = 0.007). Growing-season NDVI, reported separately as an aggregate metric, increased significantly (slope = 0.0011 $yr^{-1}$, $R^2$ = 0.584, $p < 0.001$). Summer NDVI also increased significantly (slope = 0.0006 $yr^{-1}$, $R^2$ = 0.188, $p$ = 0.030). Spring NDVI showed a positive but non-significant trend (slope = 0.0011 $yr^{-1}$, $R^2$= 0.087, $p$ = 0.152).

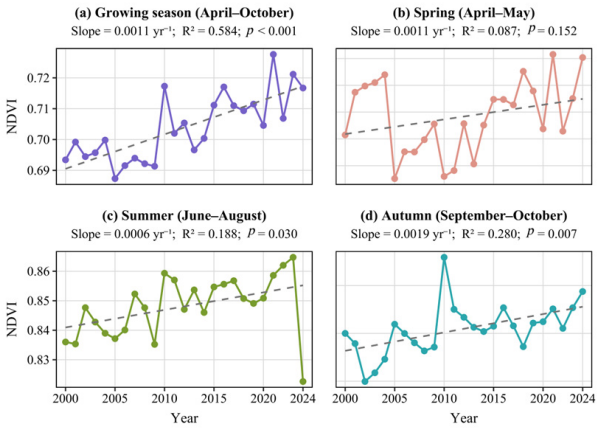


**Figure 3.** Interannual variation and linear trends in seasonal mean forest NDVI in Changbai Mountain from 2000 to 2024. The analysis was restricted to pixels retained by the fixed forest mask with at least 70% forest cover derived from the 2024 Annual China Land Cover Dataset (CLCD). Colored points and connecting lines represent annual seasonal mean NDVI, and grey dashed lines represent ordinary least-squares linear trends. The growing season (April–October) is an aggregate period comprising spring (April–May), summer (June–August), and autumn (September–October). Panel headings report the regression slope ($yr^{-1}$), coefficient of determination ($R^2$), and two-sided $p$-value. The growing-season curve summarizes the combined seasonal record and is not an independent fourth season; the individual OLS fits do not by themselves test differences among seasonal slopes. Note that the y-axis ranges differ among panels.

To further evaluate whether the differences in seasonal trends were statistically significant, a joint linear model incorporating the year × season interaction term was applied. The interaction between year and season was not significant (F = 1.131, $p$ = 0.341), providing no statistical evidence of differences among the fitted slopes in the reported model. Period-specific NDVI trend slopes were derived using the emtrends function from the emmeans R package, followed by Tukey-adjusted pairwise comparisons. Although autumn had the steepest slope, its slope did not differ significantly from those for the growing season, spring, or summer (all adjusted $p > 0.05$; Table S1). Spring NDVI displayed substantial interannual variability, as reflected by the low $R^2$ of its linear trend. Growing-season and summer NDVI generally increased over the study period, both were lower in 2024 than in 2023, with a more pronounced decline in summer. Autumn NDVI also fluctuated among years, with a notable peak in 2010, but had the largest estimated long-term slope among the seasonal series. Overall, forest greening exhibited seasonal differences in trend slopes, with autumn showing the steepest increase and spring showing a positive but non-significant trend.

### *3.2. Seasonal NDVI Correlations with Temperature and Precipitation*

NDVI–climate correlations differed among seasons (Figure 4). Spring NDVI had the highest temperature correlation among seasonal periods (r = 0.760, $p < 0.001$), whereas its correlation with precipitation was negative but not statistically significant (r = −0.299, $p$ = 0.146). Growing-season NDVI was positively correlated with temperature (r = 0.405, $p$ = 0.045), whereas its correlation with precipitation was positive but not statistically significant (r = 0.342, $p$ = 0.094).

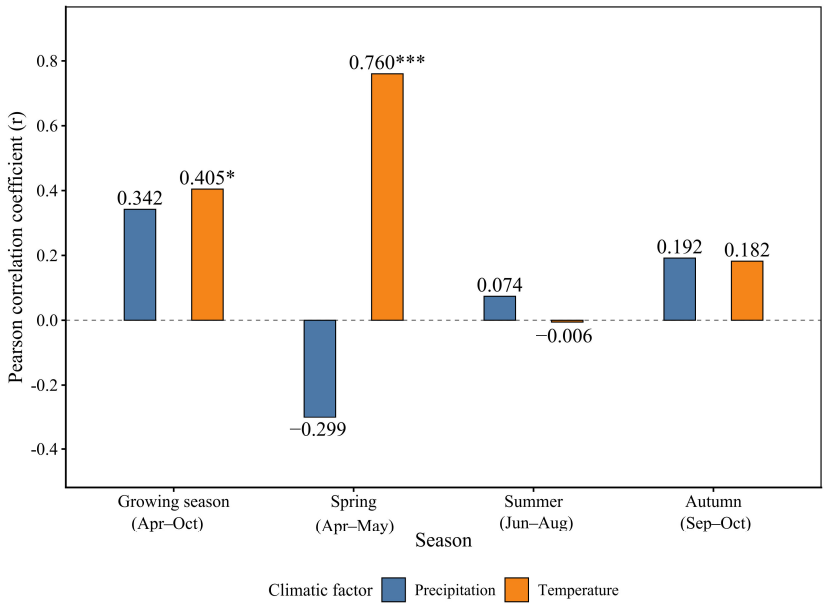


**Figure 4.** Pearson correlations between seasonal mean forest NDVI and concurrent temperature and precipitation in Changbai Mountain from 2000 to 2024. Bars represent Pearson correlation coefficients calculated from 25 paired annual observations. Blue and orange bars indicate correlations with precipitation and temperature, respectively. The dashed horizontal line denotes zero correlation ($r = 0$). Asterisks indicate statistical significance: * indicates ($p < 0.05$), and *** indicates ($p < 0.001$). Seasons were defined as the growing season (April–October), spring (April–May), summer (June–August), and autumn (September–October). The analysis was restricted to pixels classified as forest with ≥70% forest cover based on the 2024 CLCD.

In summer, NDVI showed near-zero correlations with temperature (r = −0.006, $p = 0.978$) and weak positive correlation with precipitation (r = 0.074, $p = 0.725$). In autumn, NDVI showed weak positive correlations with precipitation (r = 0.192, $p = 0.358$) and temperature (r = 0.182, $p = 0.383$). Significant NDVI–temperature correlations were detected only in spring and the growing season, whereas NDVI–precipitation correlations were not statistically significant in any seasonal period.

### *3.3. Elevation-Dependent Climate Associations with Seasonal Forest Greenness*

Elevation-stratified analyses showed that NDVI–climate correlations varied among seasons and elevation zones (Figure 5). In spring, NDVI was positively correlated with temperature across all elevation zones, with significant correlations at low (r = 0.543, $p < 0.01$), middle (r = 0.846, $p < 0.001$), and high elevations (r = 0.769, $p < 0.001$). The correlation coefficient was numerically highest at middle elevation. In contrast, spring NDVI–precipitation correlations were negative at low (r = −0.188), middle (r = −0.343), and high elevations (r = −0.390), but none were statistically significant (all $p > 0.05$).

During the growing season, NDVI–temperature correlations were positive across elevation zones, with coefficients of r = 0.367, 0.409, and 0.319 at low, middle, and high elevations, respectively. Only the middle-elevation correlation was statistically significant ($p < 0.05$). Growing-season NDVI–precipitation correlations were also positive, with coefficients of r = 0.393, 0.196, and 0.150 across low, middle, and high elevations, respectively. In summer, NDVI–temperature correlations ranged from −0.086 to 0.057, whereas NDVI–precipitation correlations ranged from 0.043 to 0.129; none were statistically significant (all $p > 0.05$). In autumn, temperature correlations ranged from 0.096 to 0.235 and precipitation correlations ranged from 0.162 to 0.187, with no statistically significant correlations detected (all $p > 0.05$).

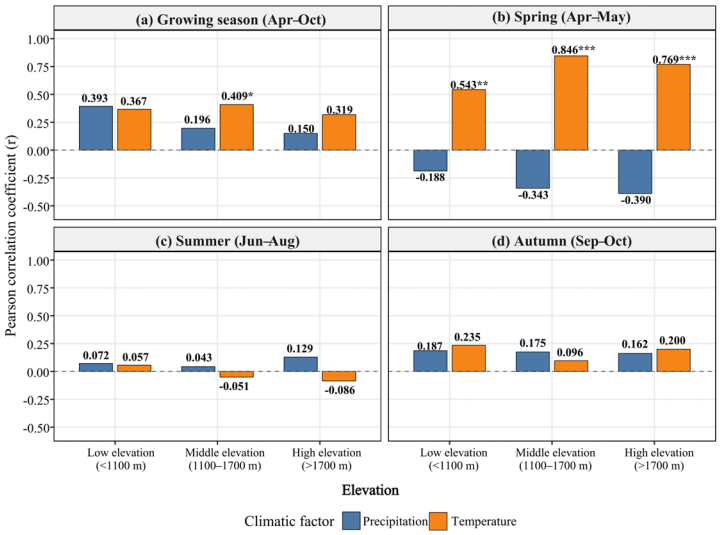


**Figure 5.** Elevation-stratified Pearson correlations between seasonal mean forest NDVI and concurrent temperature and precipitation in Changbai Mountain from 2000 to 2024. Correlations are shown for (**a**) the growing season (April–October), (**b**) spring (April–May), (**c**) summer (June–August), and (**d**) autumn (September–October) across low (<1100 m), middle (1100–1700 m), and high (>1700 m) elevation zones. Blue and orange bars represent correlations with precipitation and temperature, respectively, and the horizontal dashed line denotes $r = 0$. Numbers indicate Pearson correlation coefficients. Asterisks denote statistical significance: * indicates $p < 0.05$, ** indicates $p < 0.01$, and *** indicates $p < 0.001$. Each correlation was calculated from 25 paired annual observations. The analysis was restricted to pixels with ≥70% forest cover based on the 2024 CLCD.

Multiple regression models showed low multicollinearity between temperature and precipitation predictors (all VIFs ≤ 1.22; Figure 5). The relative magnitudes of standardized temperature and precipitation coefficients across seasons and elevation zones are shown in Figure 6. In spring, the relative magnitudes of standardized temperature coefficients were 97.8%, 93.6%, and 84.1% at low, middle, and high elevations, respectively, whereas precipitation coefficients showed corresponding magnitudes of 2.2%, 6.4%, and 15.9%.

During the growing season, the relative magnitudes of standardized temperature coefficients were 48.2%, 67.0%, and 66.9% at low, middle, and high elevations, respectively, while precipitation coefficients showed corresponding magnitudes of 51.8%, 33.0%, and 33.1%. In summer, precipitation coefficients showed larger relative magnitudes at low (57.1%) and high elevations (59.1%), whereas temperature coefficients showed a larger relative magnitude at middle elevation (53.6%). In autumn, standardized temperature and precipitation coefficients showed similar relative magnitudes. Temperature coefficients were 53.0%, 42.6%, and 52.6% at low, middle, and high elevations, respectively, while precipitation coefficients were 47.0%, 57.4%, and 47.4%.

### *3.4. Temporal Variation in Spring NDVI Correlations with Temperature and Precipitation*

The five-year sliding-window analysis suggested temporal variation in spring NDVI–climate correlations across elevation zones (Figure 7). Each window included five annual observations, with adjacent windows sharing four years; therefore, these estimates represent exploratory temporal patterns. Spring NDVI–temperature correlations were predominantly positive throughout the study period, although their magnitudes varied among elevation zones and windows. Temperature correlations were generally higher at middle and high elevations than at low elevation, with lower values occurring in several windows centred on the mid-2010s at high elevation.

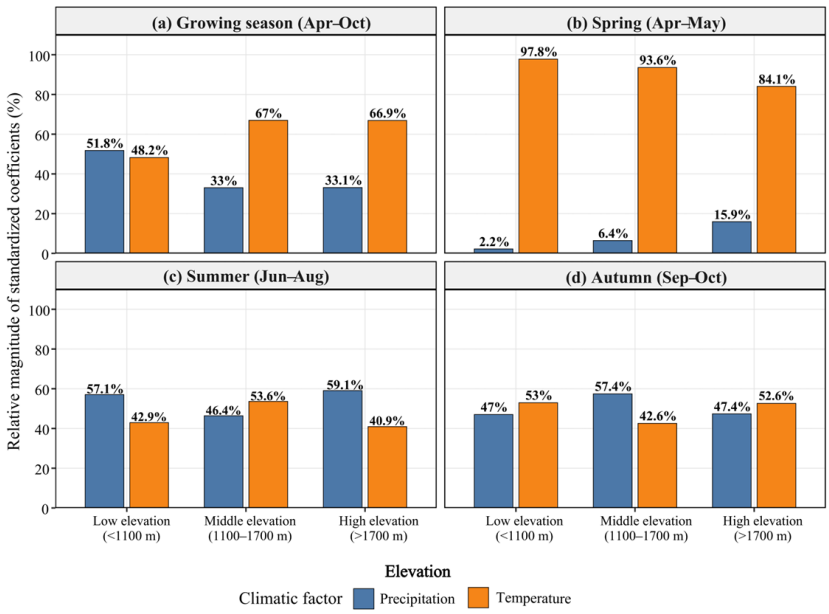


**Figure 6.** Relative magnitudes of standardized temperature and precipitation coefficients in seasonal forest NDVI regression models across elevation zones. Panels show (**a**) the growing season (April–October), (**b**) spring (April–May), (**c**) summer (June–August), and (**d**) autumn (September–October) across low (<1100 m), middle (1100–1700 m), and high (>1700 m) elevation zones. Blue and orange bars represent precipitation and temperature coefficients, respectively. Values were calculated as the absolute standardized coefficient of each climatic factor divided by the sum of the absolute standardized coefficients of both factors. These values represent the relative magnitude of standardized coefficients within each regression model and should not be interpreted as independent contributions to explained variance or causal effects on NDVI variability. Each regression was based on 25 annual observations.

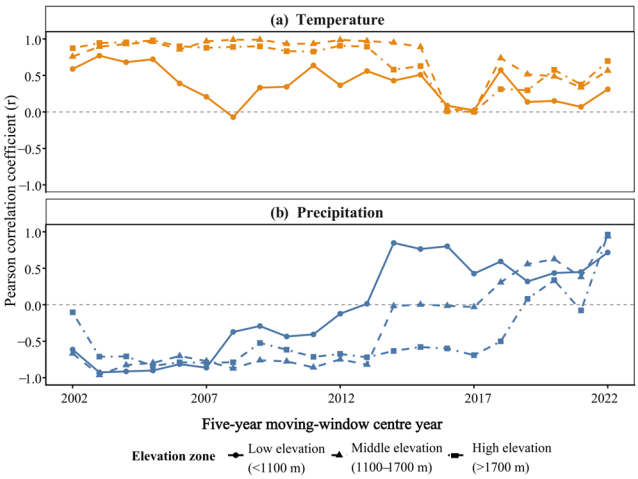


**Figure 7.** Five-year sliding-window Pearson correlations between spring mean forest NDVI and climate variables across elevation zones in Changbai Mountain from 2000 to 2024. Panels (**a**,**b**) show correlations with temperature and precipitation, respectively, for low (<1100 m), middle (1100–1700 m), and high (>1700 m) elevation zones. Each point represents the Pearson correlation coefficient for the corresponding five-year moving window, with the center year indicating the window period. Orange and blue lines represent temperature and precipitation correlations, respectively. Line types and symbols indicate elevation zones: solid lines with circles represent low elevation, dashed lines with triangles represent middle elevation, and dash-dotted lines with squares represent high elevation. Each correlation estimate was based on five annual observations, and adjacent windows shared four years; therefore, the curves are exploratory and should not be interpreted as evidence of temporal shifts in climate–NDVI relationships.

Spring NDVI–precipitation correlations showed greater variation in both magnitude and direction among windows. At low and middle elevations, precipitation correlations were mainly negative in earlier windows but approached zero or became positive in later windows. At high elevation, precipitation correlations were predominantly negative in earlier and middle windows, with some later windows showing values closer to zero or positive.

The ten-year sliding-window analysis showed partial agreement with the five-year analysis (Supplementary Figure S1). Temperature correlations were positive at middle and high elevations, whereas precipitation correlations became positive in later windows at low and middle elevations. However, high-elevation precipitation correlations remained negative across all ten-year windows, whereas the final five-year window showed a positive correlation.

### *3.5. Elevation-Dependent Associations Between Nighttime Light Intensity and Growing-Season NDVI*

The association between annual mean nighttime light (NTL) intensity and mean growing-season NDVI differed among elevation zones (Figure 8). In the low-elevation zone, NTL intensity was positively and significantly associated with growing-season NDVI, representing the only statistically significant association among the three elevation zones (slope = 0.159, $R^2$ = 0.198, $p$ = 0.026). In the middle-elevation zone, the association was positive but not statistically significant (slope = 0.438, $R^2$ = 0.049, $p$ = 0.288). In the high-elevation zone, the association was negative and not statistically significant, explaining almost no variance (slope = −0.514, $R^2$ = 0.002, $p$ = 0.853).

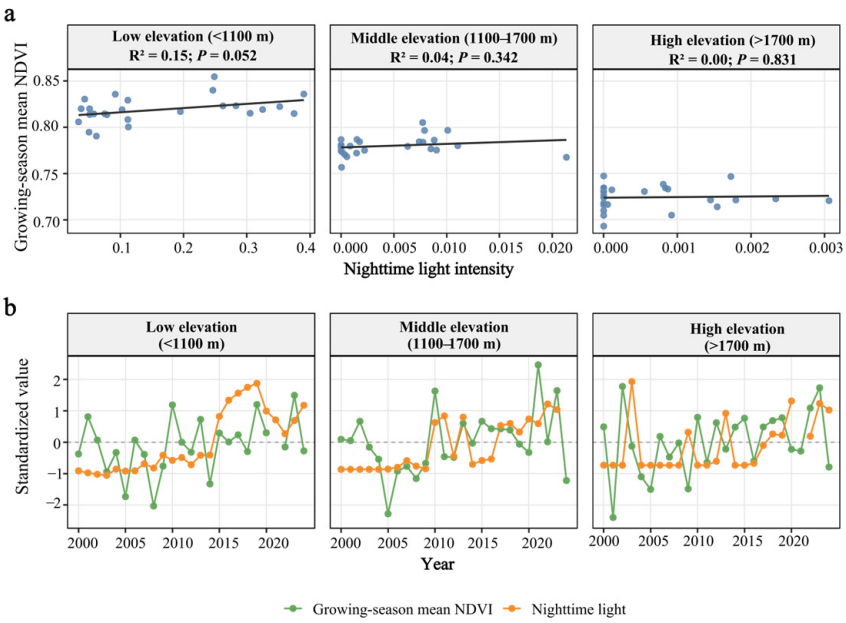


**Figure 8.** Elevation-dependent relationships between annual mean nighttime light (NTL) intensity and mean growing-season NDVI in Changbai Mountain from 2000 to 2024. (**a**) The upper panels show linear regression relationships between NTL intensity and growing-season NDVI across low (1700 m) elevation zones. The $R^2$ and $p$ values are shown in each panel. (**b**) The lower panels show standardized time-series variations in growing-season mean NDVI and NTL intensity within each elevation zone. Green and orange lines represent growing-season mean NDVI and NTL intensity, respectively. Standardized values were calculated separately within each elevation zone to facilitate comparison of interannual variation.

Standardized time-series comparisons showed contrasting temporal patterns among elevation zones. In the low-elevation zone, NTL intensity exhibited an increasing trend,

particularly during the later years of the study period, whereas mean growing-season NDVI showed a weaker increase. In the middle-elevation zone, both NTL intensity and NDVI displayed interannual fluctuations, while NTL intensity remained consistently low in the high-elevation zone.

Overall, the relationship between NTL intensity and growing-season NDVI varied across elevation zones. A significant positive association was detected only in the low-elevation zone, whereas relationships at middle and high elevations were weak and non-significant. These results indicate that the strength and direction of the NTL–NDVI association differed among elevation zones.

## 4. Discussion

### *4.1. Contrasting Spring and Autumn Greening Responses*

Vegetation greening has been widely reported, but seasonal responses can differ because spring onset and autumn senescence respond differently to environmental conditions [2,32–34]. In this study, seasonal NDVI analysis within the fixed 2024 forest footprint of Changbai Mountain revealed contrasting spring and autumn patterns: spring NDVI was strongly associated with temperature but showed no significant long-term trend, whereas autumn exhibited the largest estimated long-term increase but weak relationships with concurrent climate variables.

Spring NDVI showed a strong positive association with temperature across all elevation zones (regional $r = 0.760$, $p < 0.001$), with the strongest relationship at middle elevation ($r = 0.846$, $p < 0.001$). However, spring NDVI showed no significant long-term trend (slope = 0.0011 $yr^{-1}$, $p = 0.152$). Spring vegetation activity in temperate ecosystems is closely linked to temperature-driven phenological processes, particularly the timing of leaf emergence and spring growth [35,36], and the strong association observed here is consistent with this pattern. Our results indicate that temperature sensitivity mainly reflects interannual variability in spring greenness rather than a persistent long-term increase. In Changbai Mountain, snow cover duration, late frost events, and soil thawing processes may contribute to the absence of a sustained spring greening trend [3,8]. The stronger temperature association at middle elevation suggests that spring vegetation responses are not simply determined by colder conditions at higher elevations, but may reflect the combined effects of thermal conditions, snow dynamics, and local forest characteristics.

Autumn exhibited the largest estimated long-term NDVI slope among the seasonal periods (0.0019 $yr^{-1}$, $p = 0.007$), whereas its correlations with concurrent autumn temperature ($r = 0.182$, $p = 0.383$) and precipitation ($r = 0.192$, $p = 0.358$) were not significant. Previous studies have documented delayed autumn senescence and enhanced late-season vegetation activity in temperate forests, partly associated with warming-induced phenological changes and growing-season extension [37–39]. These studies document autumn greening; our results show that the long-term autumn increase was not associated with concurrent climate variability. This decoupling suggests that autumn greening may reflect processes beyond concurrent climate variability, including phenological adjustments and lagged effects of previous-season environmental conditions [37,38,40,41]. Changes in forest structure may also contribute to long-term satellite-derived greenness trends [11].

The spring–autumn contrast indicates that seasonal decomposition provides information that annual or growing-season averages may obscure. Because the year × season interaction and Tukey-adjusted pairwise comparisons did not indicate significant differences among seasonal slopes, these contrasts represent differences in estimated trend magnitude rather than statistically confirmed differences among seasons. Nevertheless, spring and autumn greenness changes showed different relationships with climate variability and long-term trends: spring NDVI was more closely associated with interannual

temperature variability, whereas autumn showed a stronger long-term increasing trend despite weak relationships with concurrent climate variables.

### *4.2. Non-Monotonic Elevational Pattern of Spring NDVI–Temperature Associations*

Mountain vegetation responses are often expected to show stronger temperature constraints at higher elevations because colder conditions increase thermal limitations [1]. However, elevational patterns of vegetation–climate associations are not necessarily linear and can be modified by local environmental conditions [5,14]. In Changbai Mountain, spring NDVI–temperature associations showed a non-monotonic pattern across elevation zones. Positive correlations were observed at all elevations, with the highest correlation at middle elevation ($r = 0.846$, $p < 0.001$), followed by high elevation ($r = 0.769$, $p < 0.001$) and low elevation ($r = 0.543$, $p < 0.01$). This pattern differs from the expectation that stronger thermal limitation at higher elevations would necessarily correspond to stronger NDVI–temperature associations [1].

Previous studies in Changbai Mountain have shown that spring vegetation development is jointly associated with temperature conditions and snow cover dynamics. Chang et al. (2023) reported that spring forest phenology was influenced by both spring temperature and snow cover conditions [3], while Chang et al. (2024) demonstrated that snow cover seasonality affected the timing of spring vegetation development [8]. The relatively high NDVI–temperature association at middle elevation may be consistent with a transitional environmental setting where both thermal conditions and snow-related processes influence spring vegetation activity. However, these mechanisms were not directly measured in this study. The stronger association at middle elevation may therefore reflect the combined effects of temperature variability and other elevation-dependent environmental constraints rather than elevation itself.

The lower association at low elevation may be related to reduced thermal limitation under warmer conditions. When temperature becomes less limiting, other unmeasured environmental factors may contribute more strongly to interannual NDVI variability. At high elevation, the relatively high NDVI–temperature association indicates that interannual temperature variability remains closely linked with spring vegetation activity. However, the absence of a further increase compared with middle elevation suggests that stronger thermal constraints do not necessarily produce stronger NDVI–temperature associations. Additional factors, including snow duration and shorter growing seasons, may limit further increases in temperature coupling toward higher elevations [1,5,8].

The elevational pattern observed here indicates that spring vegetation–temperature associations in Changbai Mountain cannot be inferred from thermal limitation alone. Instead, within-mountain heterogeneity in temperature conditions, snow-related processes, and local environmental characteristics should be considered when interpreting remotely sensed vegetation variability in mountain ecosystems [42,43]. Although the correlation was numerically highest at middle elevation, formal comparisons among correlation coefficients are required to determine whether these differences are statistically significant.

### *4.3. Temporal Variability in Climate–Greenness Relationships*

Climate–vegetation relationships are not necessarily stationary over time, and temporal variations in vegetation responses under changing climatic conditions and environmental disturbances have been reported [15,28,30,44]. In mountain ecosystems, these variations may be associated with multiple environmental constraints, including temperature variability, snow dynamics, and seasonal processes [1,5,8].

The five-year moving-window analysis suggested temporal variations in spring climate–greenness associations across elevation zones. Spring NDVI–temperature correla-

tions remained positive in most windows, consistent with a relatively persistent association between interannual temperature variability and spring vegetation activity. However, the strength of these correlations varied among periods, with weaker estimates centred on the mid-2010s, particularly in some high-elevation windows. In contrast, precipitation associations showed stronger temporal fluctuations, shifting from predominantly negative correlations during the early study period toward neutral or positive correlations in later windows, especially at low and middle elevations. Because each moving window contained five annual observations and adjacent windows shared four overlapping years, these temporal patterns are interpreted as exploratory variations in climate–greenness associations rather than confirmed long-term shifts.

The ten-year moving-window analysis showed partial agreement with the five-year results. Temperature–NDVI associations remained positive across elevation zones over the longer temporal scale, whereas precipitation correlations were more sensitive to window length. For example, precipitation correlations at high elevation became positive in the final five-year window but remained negative throughout the ten-year analysis. This difference suggests that temperature associations were more stable across window lengths, whereas precipitation associations were more sensitive to the analysis window.

Temporal variation in spring climate–greenness associations may be related to variations in early-season environmental conditions. Previous studies in Changbai Mountain have shown that spring vegetation activity is associated with temperature and snow cover dynamics, with snowmelt timing linked to vegetation onset [3,8]. Changes in snow duration, freeze–thaw conditions, and precipitation regimes could contribute to variations in the strength of these climate–greenness associations, although these processes were not directly evaluated in this study.

Together, the five-year and ten-year analyses suggest that climate–greenness relationships in Changbai Mountain may vary across temporal scales. Temperature showed relatively consistent positive associations with spring NDVI, whereas precipitation relationships were more sensitive to window length. These results suggest that climate–greenness associations should be assessed across multiple temporal scales when interpreting remotely sensed vegetation responses in mountain ecosystems.

### *4.4. Spatial Heterogeneity of Human Activity–Greenness Associations Across Elevation Zones*

Nighttime light (NTL) intensity has been widely used as an indicator of human activity intensity and has been applied to examine potential relationships between anthropogenic signals and vegetation dynamics [16–18]. However, associations between human activity indicators and vegetation greenness can vary spatially because human activities are unevenly distributed across landscapes.

In Changbai Mountain, the association between NTL intensity and growing-season NDVI differed among elevation zones. A significant positive association was detected only at low elevation ($R^2 = 0.198$, $p = 0.026$), whereas no significant associations were observed at middle or high elevations. Because both NTL intensity and NDVI may contain long-term temporal trends during 2000–2024, this raw association should be interpreted as a broad spatial–temporal correspondence rather than evidence of year-to-year covariation between human activity and forest greenness [45].

This low-elevation association may be related to greater accessibility and higher human activity intensity in these areas. Low-elevation forests are generally closer to human settlements and infrastructure, where changes in human activity indicators may coincide with broader regional changes. However, the positive association does not indicate that human activities directly enhanced vegetation greenness, because NTL intensity and NDVI may respond simultaneously to shared socioeconomic and environmental changes.

In contrast, the absence of significant NTL–NDVI associations at middle and high elevations suggests that vegetation variability in these zones was less strongly associated with anthropogenic activity indicators. Higher-elevation forests generally have lower human accessibility and stronger climatic constraints, and vegetation dynamics may be more closely related to temperature, snow conditions, and other natural environmental factors. This spatial pattern is consistent with previous studies showing that human activity–vegetation associations are often concentrated in accessible low-elevation areas, whereas remote mountain ecosystems are more strongly associated with climatic variability [16–18].

Overall, the NTL–NDVI associations varied among elevation zones. Low-elevation forests showed a significant raw association between NTL intensity and NDVI, whereas middle- and high-elevation forests showed no significant relationships. These results suggest that human activity indicators should be interpreted together with elevation-related environmental heterogeneity when assessing vegetation dynamics in mountain ecosystems.

### *4.5. Methodological Considerations and Future Research*

This study focused on historical forest greenness trajectories within a consistent forest domain identified by the 2024 CLCD forest mask. Therefore, the analysis characterized long-term NDVI variations within currently forest-dominated areas rather than annual changes in forest extent during 2000–2024. This approach provided spatial consistency among years and reduced potential interference from non-forest surfaces. However, because a fixed forest mask was applied throughout the study period, the analysis does not distinguish persistent forest areas from possible historical land-cover transitions. Future studies incorporating annual land-cover products could further improve the separation of forest persistence and vegetation change processes. In addition, the 1 km spatial resolution of MOD13A3 represents integrated canopy conditions within pixels, and higher-resolution remote sensing products could provide additional insights into vegetation responses at finer spatial scales.

Temperature and precipitation captured the major seasonal climatic conditions associated with forest greenness changes, but they do not represent all environmental processes affecting mountain vegetation dynamics. Snow conditions, radiation, soil moisture, soil temperature, and atmospheric water demand can influence the timing and intensity of vegetation responses, particularly during spring canopy development, summer growth, and autumn senescence. Incorporating these environmental variables in future analyses would provide a more comprehensive understanding of seasonal climate–vegetation relationships and help further clarify the mechanisms underlying observed NDVI variations.

The statistical analyses in this study describe statistical associations among climate variables, nighttime light intensity, and NDVI variability rather than causal relationships. Pearson correlations characterize synchronous relationships between variables, whereas standardized regression coefficients represent the relative magnitude of climatic predictors within each fitted model and should not be interpreted as independent contributions to explained variance. The five-year sliding-window analysis also requires careful interpretation because each estimate was based on only five annual observations and adjacent windows shared four years. Individual anomalous years may therefore influence multiple overlapping windows. Longer observation periods and complementary approaches, such as time-varying coefficient models or change-point analyses, could provide further evidence for potential temporal changes in climate–vegetation relationships.

The interpretation of nighttime light (NTL) patterns should consider the mixed nature of artificial illumination signals. NTL intensity integrates information from multiple human-related sources, including settlements, transportation infrastructure, tourism activities, forest management activities, and changes in lighting conditions. The positive

low-elevation NTL–NDVI association observed in this study may reflect the combined influence of human activity signals and concurrent environmental changes. Because both NTL intensity and NDVI may contain long-term temporal trends during 2000–2024, this raw association should be interpreted as a broad spatial–temporal correspondence rather than year-to-year covariation. Future studies integrating land-use dynamics, infrastructure data, tourism intensity, and forest management records could provide further insight into the mechanisms underlying NTL–vegetation relationships.

Elevation-based analyses showed variation in climate–NDVI relationships among elevation zones; however, elevation also integrates multiple environmental and human gradients, including temperature, snow conditions, forest composition, terrain characteristics, and accessibility. Future studies incorporating forest types, topographic variables, snow dynamics, and disturbance information could further resolve spatial heterogeneity in vegetation responses. Nevertheless, the seasonal framework adopted in this study highlights differences among spring canopy development, summer growth conditions, and autumn vegetation decline, providing additional context for understanding long-term forest greenness changes in Changbai Mountain.

## 5. Conclusions

Within the 2024 forest mask of Changbai Mountain, forest greenness exhibited seasonal and elevational patterns during 2000–2024 that were not captured by growing-season averages alone. Seasonal greenness trends and climate associations showed contrasting patterns. Autumn showed the largest estimated NDVI increase, yet neither temperature nor precipitation showed significant associations with autumn NDVI. Spring, in contrast, showed the highest temperature correlation among seasons despite the absence of a significant long-term trend. This pattern indicates that strong interannual climate associations do not necessarily translate into persistent long-term greening trends, and that the factors associated with multi-year greenness changes may differ from those associated with year-to-year variability.

Spring NDVI–temperature correlations were positive across all elevation zones, with the largest coefficient observed at middle elevation rather than at the highest sites. This pattern suggests that factors beyond temperature alone influence the strength of spring greenness–climate coupling. Five-year sliding-window analyses suggested temporal variation in spring NDVI–climate correlations, and partial agreement between five-year and ten-year windows further indicates that these relationships are sensitive to the temporal scale of analysis. The NTL–NDVI association was significant only at low elevation and should be interpreted as a broad spatial–temporal correspondence rather than evidence of a causal relationship, because both NTL and NDVI may contain shared long-term trends.

These findings show that forest greenness dynamics in Changbai Mountain are seasonally asymmetric, elevation-dependent, and sensitive to temporal scale. Mountain forest greenness is better interpreted by jointly considering season, elevation, temporal scale, and the spatial context of landscape-scale human activity indicators.

**Supplementary Materials:** The following supporting information can be downloaded at: https://www.mdpi.com/article/10.3390/rs18213630/s1, Table S1: Statistical evaluation of seasonal NDVI trend differences using a year × season interaction model; Figure S1: Ten-year sliding-window Pearson correlations between spring mean forest NDVI and climate variables across elevation zones in Changbai Mountain from 2000 to 2024.

**Author Contributions:** Conceptualization, Y.W. and Z.Z.; methodology, Y.W.; software, Y.W.; formal analysis, Y.W.; investigation, Y.W.; data curation, Y.W.; visualization, Y.W.; writing—original draft

preparation, Y.W.; writing—review and editing, Z.Z., Z.L. and C.F.; supervision, Z.Z. All authors have read and agreed to the published version of the manuscript.

**Funding:** This research was funded by the Science and Technology Projects of Xizang Autonomous Region, China, grant number XZ202501ZY0091, and the National Key R&D Program of China, grant numbers 2024YFF1307800, 2024YFF1307801 and 2025YFF1702504.

**Data Availability Statement:** The MODIS/Terra MOD13A3 V061 NDVI data are publicly available from the NASA Land Processes Distributed Active Archive Center (LP DAAC; https://doi.org/10.5067/MODIS/MOD13A3.061). The ASTER GDEM V003 data are publicly available from NASA LP DAAC (https://doi.org/10.5067/ASTER/ASTGTM.003). The Annual China Land Cover Dataset (CLCD v01, Version 1.0.4) is publicly available from Zenodo (https://doi.org/10.5281/zenodo.15853565). The 1 km monthly precipitation dataset for China (1901–2024) is publicly available from Zenodo (https://doi.org/10.5281/zenodo.3114194). The 1 km monthly mean temperature dataset for China (1901–2024) is publicly available from the National Tibetan Plateau/Third Pole Environment Data Center (https://doi.org/10.11888/Meteoro.tpdc.270961). The Extended VIIRS-like Artificial Nighttime Light Dataset of China (1986–2024) is publicly available from the National Tibetan Plateau/Third Pole Environment Data Center (https://doi.org/10.11888/HumanNat.tpdc.302930). The processed data generated during this study are available from the corresponding author upon reasonable request.

**Conflicts of Interest:** The authors declare no conflicts of interest.

## References

1. Pepin, N.; Bradley, R.S.; Diaz, H.F.; Baraer, M.; Caceres, E.B.; Forsythe, N.; Fowler, H.; Greenwood, G.; Hashmi, M.Z.; Liu, X.D.; et al. Elevation-dependent warming in mountain regions of the world. *Nat. Clim. Change* **2015**, *5*, 424–430. [CrossRef]
2. Piao, S.; Liu, Q.; Chen, A.; Janssens, I.A.; Fu, Y.; Dai, J.; Liu, L.; Lian, X.; Shen, M.; Zhu, X. Plant phenology and global climate change: Current progresses and challenges. *Glob. Change Biol.* **2019**, *25*, 1922–1940. [CrossRef] [PubMed]
3. Chang, S.; He, H.S.; Huang, F.; Krohn, J. Spring temperature and snow cover co-regulate variations of forest phenology in Changbai Mountains, Northeast China. *Eur. J. For. Res.* **2023**, *143*, 547–560. [CrossRef]
4. Zhu, Z.; Piao, S.; Myneni, R.B.; Huang, M.; Zeng, Z.; Canadell, J.G.; Ciais, P.; Sitch, S.; Friedlingstein, P.; Arneth, A.; et al. Greening of the Earth and its drivers. *Nat. Clim. Change* **2016**, *6*, 791–795. [CrossRef]
5. Gao, M.; Piao, S.; Chen, A.; Yang, H.; Liu, Q.; Fu, Y.H.; Janssens, I.A. Divergent changes in the elevational gradient of vege-tation activities over the last 30 years. *Nat. Commun.* **2019**, *10*, 2970. [CrossRef] [PubMed]
6. Zhou, Y. Asymmetric Behavior of Vegetation Seasonal Growth and the Climatic Cause: Evidence from Long-Term NDVI Dataset in Northeast China. *Remote Sens.* **2019**, *11*, 2107. [CrossRef]
7. Li, M.; Wu, Z.; Qin, L.; Meng, X. Extracting vegetation phenology metrics in Changbai Mountains using an improved logistic model. *Chin. Geogr. Sci.* **2011**, *21*, 304–311. [CrossRef]
8. Chang, S.; Huang, F.; He, H.S.; Liu, K.; Krohn, J. Impacts of snow cover seasonality on spring land surface phenology of forests in Changbai mountains of Northeast China. *Sci. Total Environ.* **2024**, *927*, 171965. [CrossRef] [PubMed]
9. Ren, C.; Zhang, L.; Fu, B. Unraveling Effect of Snow Cover on Spring Vegetation Phenology across Different Vegetation Types in Northeast China. *Remote Sens.* **2023**, *15*, 4783. [CrossRef]
10. Merrick, T.; Bennartz, R.; Jorge, M.L.S.P.; Merrick, C.; Bohlman, S.A.; Silva, C.A.; Pau, S. Comparing Phenology of a Tem-perate Deciduous Forest Captured by Solar-Induced Fluorescence and Vegetation Indices. *Remote Sens.* **2023**, *15*, 5101. [CrossRef]
11. Dai, L.; Qi, L.; Wang, Q.; Su, D.; Yu, D.; Wang, Y.; Ye, Y.; Jiang, S.; Zhao, W. Changes in forest structure and composition on Changbai Mountain in Northeast China. *Ann. For. Sci.* **2011**, *68*, 889–897. [CrossRef]
12. Hou, G.; Zhang, H.; Wang, Y. Vegetation dynamics and its relationship with climatic factors in the Changbai Mountain Natural Reserve. *J. Mt. Sci.* **2011**, *8*, 865–875. [CrossRef]
13. Guo, X.-Y.; Zhang, H.-Y.; Wang, Y.-Q.; He, H.-S.; Wu, Z.-F.; Jin, Y.-H.; Zhang, Z.-X.; Zhao, J.-J. Comparison of the spa-tio-temporal dynamics of vegetation between the Changbai Mountains of eastern Eurasia and the Appalachian Mountains of eastern North America. *J. Mt. Sci.* **2018**, *15*, 1–12. [CrossRef]
14. Wang, S.; Wang, X.; Gai, X.; Zhou, L.; Zhou, W.; Han, Y.; Yu, D. Topography-dependent climatic sensitivities in spruce tree growth in the Changbai Mountain, Northeast China. *Trees* **2021**, *35*, 961–971. [CrossRef]
15. Zheng, S.; Peng, D.; Zhang, B.; Yu, L.; Pan, Y.; Wang, Y.; Feng, X.; Dou, C. Temporal variation characteristics in the association between climate and vegetation in Northwest China. *Sci. Rep.* **2024**, *14*, 17905. [CrossRef] [PubMed]

16. Zheng, Q.; Seto, K.C.; Zhou, Y.; You, S.; Weng, Q. Nighttime light remote sensing for urban applications: Progress, challenges, and prospects. *ISPRS J. Photogramm. Remote Sens.* **2023**, *202*, 125–141. [CrossRef]
17. Levin, N.; Kyba, C.C.M.; Zhang, Q.; Sánchez de Miguel, A.; Román, M.O.; Li, X.; Portnov, B.A.; Molthan, A.L.; Jechow, A.; Miller, S.D.; et al. Remote sensing of night lights: A review and an outlook for the future. *Remote Sens. Environ.* **2020**, *237*, 111443. [CrossRef]
18. Chen, X.; Nordhaus, W.D. Using luminosity data as a proxy for economic statistics. *Proc. Natl. Acad. Sci. USA* **2011**, *108*, 8589–8594. [CrossRef] [PubMed]
19. Didan, K. *NASA Land Processes Distributed Active Archive Center*; NASA: Washington, DC, USA, 2021. [CrossRef]
20. Huete, A.; Didan, K.; Miura, T.; Rodriguez, E.P.; Gao, X.; Ferreira, L.G. Overview of the radiometric and biophysical per-formance of the MODIS vegetation indices. *Remote Sens. Environ.* **2002**, *83*, 195–213. [CrossRef]
21. Peng, S. *1-km Monthly Mean Temperature Dataset for China (1901–2024)*; National Tibetan Plateau Data Center: Beijing, China, 2025. [CrossRef]
22. Peng, S. 1-km monthly precipitation dataset for China (1901–2024). *Earth Syst. Sci. Data* **2025**, *11*, 1931–1946. [CrossRef]
23. Tian, Y.; Zheng, J.; Zhang, Z.; Zhang, T.; Xu, B. *Extended VIIRS-Like Artificial Nighttime Night Dataset of China (1986–2024)*; National Tibetan Plateau Data Center: Beijing, China, 2025. [CrossRef]
24. Yang, J.; Huang, X. The 30 m annual land cover datasets and its dynamics in China from 1985 to 2024. *Earth Syst. Sci. Data* **2025**, *13*, 3907–3925. [CrossRef]
25. NASA/METI/AIST/Japan Spacesystems; U.S./Japan ASTER Science Team. *ASTER Global Digital Elevation Model V003*; NASA: Washington, DC, USA, 2019. [CrossRef]
26. Bartold, M. Development of forest cover mask to monitor the health condition of forests in Poland using long-term satellite observations. *For. Res. Pap.* **2016**, *77*, 141–150. [CrossRef]
27. Hansen, M.C.; Potapov, P.V.; Moore, R.; Hancher, M.; Turubanova, S.A.; Tyukavina, A.; Thau, D.; Stehman, S.V.; Goetz, S.J.; Loveland, T.R.; et al. High-resolution global maps of 21st-century forest cover change. *Science* **2013**, *342*, 850–853. [CrossRef] [PubMed]
28. Forkel, M.; Carvalhais, N.; Verbesselt, J.; Mahecha, M.D.; Neigh, C.S.R.; Reichstein, M. Trend change detection in NDVI time series: Effects of inter-annual variability and methodology. *Remote Sens.* **2013**, *5*, 2113–2144. [CrossRef]
29. Dormann, C.; Elith, J.; Bacher, S.; Buchmann, C.; Carl, G.; Carré, G.; Diekötter, T.; García Márquez, J.; Gruber, B.; Lafourcade, B.; et al. Collinearity: A review of methods to deal with it and a simulation study evaluating their performance. *Ecography* **2013**, *36*, 27–46. [CrossRef]
30. Verbesselt, J.; Hyndman, R.; Newnham, G.; Culvenor, D. Detecting trend and seasonal changes in satellite image time series. *Remote Sens. Environ.* **2010**, *114*, 106–115. [CrossRef]
31. Elvidge, C.D.; Baugh, K.; Zhizhin, M.; Hsu, F.C.; Ghosh, T. VIIRS night-time lights. *Int. J. Remote Sens.* **2017**, *38*, 5860–5879. [CrossRef]
32. Yin, H.; Liu, Q.; Liao, X.; Ye, H.; Li, Y.; Ma, X. Refined Analysis of Vegetation Phenology Changes and Driving Forces in High Latitude Altitude Regions of the Northern Hemisphere: Insights from High Temporal Resolution MODIS Products. *Remote Sens.* **2024**, *16*, 1744. [CrossRef]
33. Chen, C.; Park, T.; Wang, X.; Piao, S.; Xu, B.; Chaturvedi, R.K.; Fuchs, R.; Brovkin, V.; Ciais, P.; Fensholt, R.; et al. China and India lead in greening of the world through land-use management. *Nat. Sustain.* **2019**, *2*, 122–129. [CrossRef] [PubMed]
34. Jeong, S.J.; Ho, C.H.; Gim, H.J.; Brown, M.E. Phenology shifts at start vs. end of growing season in temperate vegetation over the Northern Hemisphere. *Glob. Change Biol.* **2011**, *17*, 2385–2399. [CrossRef]
35. Chang, C.-T.; Chiang, J.-M.; Huang, C.-Y. Delineating Forest Canopy Phenology: Insights from Long-Term Phenocam Observations in North America. *Remote Sens.* **2025**, *17*, 2893. [CrossRef]
36. Fu, Y.H.; Piao, S.; Vitasse, Y.; Zhao, H.; De Boeck, H.J.; Liu, Q.; Yang, H.; Weber, U.; Hänninen, H.; Janssens, I.A. Increased activity of vegetation growth and carbon uptake in spring explains recent changes in spring phenology. *Glob. Change Biol.* **2014**, *20*, 1172–1185. [CrossRef] [PubMed]
37. Zohner, C.M.; Mirzagholi, L.; Renner, S.S.; Mo, L.; Rebindaine, D.; Bucher, R.; Palouš, D.; Vitasse, Y.; Fu, Y.H.; Stocker, B.D.; et al. Effect of climate warming on the timing of autumn leaf senescence reverses after the summer solstice. *Science* **2023**, *381*, eadf5098. [CrossRef] [PubMed]
38. Zhang, Y.; Hong, S.; Liu, Q.; Huntingford, C.; Peñuelas, J.; Rossi, S.; Myneni, R.B.; Piao, S. Autumn canopy senescence has slowed down with global warming since the 1980s in the Northern Hemisphere. *Commun. Earth Environ.* **2023**, *4*, 173. [CrossRef]
39. Keenan, T.F.; Gray, J.; Friedl, M.A.; Toomey, M.; Bohrer, G.; Hollinger, D.Y.; Munger, J.W.; O'Keefe, J.; Schmid, H.P.; Wing, I.S.; et al. Net carbon uptake has increased through warming-induced changes in temperate forest phenology. *Nat. Clim. Change* **2014**, *4*, 598–604. [CrossRef]
40. Liu, L.; Zhang, Y.; Wu, S.; Li, S.; Qin, D. Water memory effects and their impacts on global vegetation productivity and re-silience. *Sci. Rep.* **2018**, *8*, 2962. [CrossRef] [PubMed]

41. Chen, Z.; Wang, W.; Fu, J. Vegetation response to precipitation anomalies under different climatic and biogeographical con-ditions in China. *Sci. Rep.* **2020**, *10*, 830. [CrossRef] [PubMed]
42. Charrière, D.; Francon, L.; Giuliani, G. NDVI or PPI: A (Quick) Comparison for Vegetation Dynamics Monitoring in Moun-tainous Area. *Remote Sens.* **2024**, *16*, 3894. [CrossRef]
43. Wright, T.E.; Chikamoto, Y.; Birch, J.D.; Lutz, J.A. Remote Sensing Detection of Growing Season Freeze-Induced Defoliation of Montane Quaking Aspen (Populus tremuloides) in Southern Utah, USA. *Remote Sens.* **2024**, *16*, 3477. [CrossRef]
44. Ummenhofer, C.C.; Meehl, G.A. Extreme weather and climate events with ecological relevance: A review. *Philos. Trans. R. Soc. B Biol. Sci.* **2017**, *372*, 20160135. [CrossRef] [PubMed]
45. Granger, C.W.J.; Newbold, P. Spurious regressions in econometrics. *J. Econom.* **1974**, *2*, 111–120. [CrossRef]

**Disclaimer/Publisher's Note:** The statements, opinions and data contained in all publications are solely those of the individual author(s) and contributor(s) and not of MDPI and/or the editor(s). MDPI and/or the editor(s) disclaim responsibility for any injury to people or property resulting from any ideas, methods, instructions or products referred to in the content.